

Rothamsted Repository Download

A - Papers appearing in refereed journals

Gholami, H., TakhtiNajad, E. J., Collins, A. L. and Fathabadi, A. 2019. Monte Carlo fingerprinting of the terrestrial sources of different particle size fractions of coastal sediment deposits using geochemical tracers: some lessons for the user community. *Environmental Science and Pollution Research*. 26 (13), pp. 13560-13579.

The publisher's version can be accessed at:

- <https://dx.doi.org/10.1007/s11356-019-04857-0>

The output can be accessed at: <https://repository.rothamsted.ac.uk/item/8wqx5>.

© 17 March 2019, Rothamsted Research. Licensed under the Creative Commons CC BY.



Monte Carlo fingerprinting of the terrestrial sources of different particle size fractions of coastal sediment deposits using geochemical tracers: some lessons for the user community

Hamid Gholami¹ · Ebrahim Jafari TakhtiNajad¹ · Adrian L. Collins² · Aboalhasan Fathabadi³

Received: 16 November 2018 / Accepted: 13 March 2019 / Published online: 26 March 2019
© Springer-Verlag GmbH Germany, part of Springer Nature 2019

Abstract

A sediment source fingerprinting method, including a Monte Carlo simulation framework, was used to quantify the contributions of terrestrial sources of fine- (< 63 μm) and coarse-grained (63–500 μm) sediments sampled from three categories of coastal sediment deposits in the Jagin catchment, south-east of Jask, Hormozgan province, southern Iran: coastal dunes (CD), terrestrial sand dunes or onshore sediments (TSD), and marine or offshore sediments (MD). Forty-nine geochemical properties were measured in the two size fractions and a three-stage statistical process consisting of a conservation test, the Kruskal–Wallis *H* test, and stepwise discriminant function analysis (DFA) was applied to select final composite fingerprints for terrestrial source discrimination. Based on the statistical tests, four final fingerprints comprising Be, Ni, K and Cu and seven final fingerprints consisting Cu, Th, Be, Al, La, Mg and Fe were selected for discriminating terrestrial sources of the coastal fine- and coarse-grained sediments, respectively. Two geological spatial sources, including Quaternary (clay flat, high and low level fans and valley terraces) and Palaeocene age deposits, were identified as the main terrestrial sources of the fine-grained sediment sampled from the coastal deposits. A geological spatial source consisting of sandstone with siltstone, mudstone and minor conglomerate (Palaeocene age deposits) was identified as the main terrestrial source for coarse-grained sediment sampled from the coastal deposits.

Keywords Coastal sediment fingerprinting · Monte Carlo simulation framework · Uncertainty · Iran

Introduction

Coastal sediment deposits in Iran extend from the eastern part of Jask (Hormozgan province) to Chahbahar (Sistan and Baluchestan province) with coastal plains covering an area of > 1.56 million hectares of Hormozgan province. Based on

the wind erosion map of Iran, provided by the Iran Forests, Range and Watershed Management Organization (IFRWMO), 29 terrestrial diffuse sediment sources prone to aeolian erosion comprising sand dunes, clay flats, salty land, sand sheets, bare land and abandoned agricultural areas occupy ~209,000 ha of the coastal plains. In turn, an estimated 475,000 ha of the coastal plains is impacted by the on-site and off-site consequences of the aeolian erosion of these critical dust sources. Morshedi Nodej and Rezazadeh (2018) reported that such coastal plains, and, in particular, their coastal dunes, have the highest potential to become critical sources of aeolian dust and, accordingly, on this basis, Jask has been identified as the most important source of wind erosion dust-related problems in the Hormozgan province of Iran. Since migration and erosion of coastal sand dunes by wind cause many on-site (e.g., soil degradation, depletion of soil macro- and micro-nutrients, a reduction in soil depth) and off-site problems (e.g., penetration of dust and its constituents into lungs causing respiratory disease, visibility problems during dust storms) in the study area and is a serious challenge for rural societies in

Responsible editor: Philippe Garrigues

- ✉ Hamid Gholami
hgholami@hormozgan.ac.ir
- ✉ Adrian L. Collins
adrian.collins@rothamsted.ac.uk

- ¹ Department of Natural Resources Engineering, University of Hormozgan, Bandar-Abbas, Hormozgan, Iran
- ² Sustainable Agriculture Sciences Department, Rothamsted Research, North Wyke, Okehampton, Devon EX20 2SB, UK
- ³ Department of Range and Watershed Management, University of Gonbad-e-Kavoos, Gonbad-e-Kavoos, Golestan, Iran

the east of Jask, identifying and quantifying critical sources of the dust prone to remobilization from these particular coastal sediment deposits are necessary for improved management and planning in the coastal plains.

A range of techniques has been employed for studying sediment provenance in coastal plains, with much of the focus

on using not only mineralogy (Hein et al. 2013; Kairyte and Stevens 2009; Lahijani and Tavakoli 2012; Wong et al. 2013) but also multidisciplinary approaches including a combination of geochemical tracers, direct measurements and numerical modelling (Bernard et al. 2013); radiometric analyses (Carvalho et al. 2013); elemental and mineralogical analyses

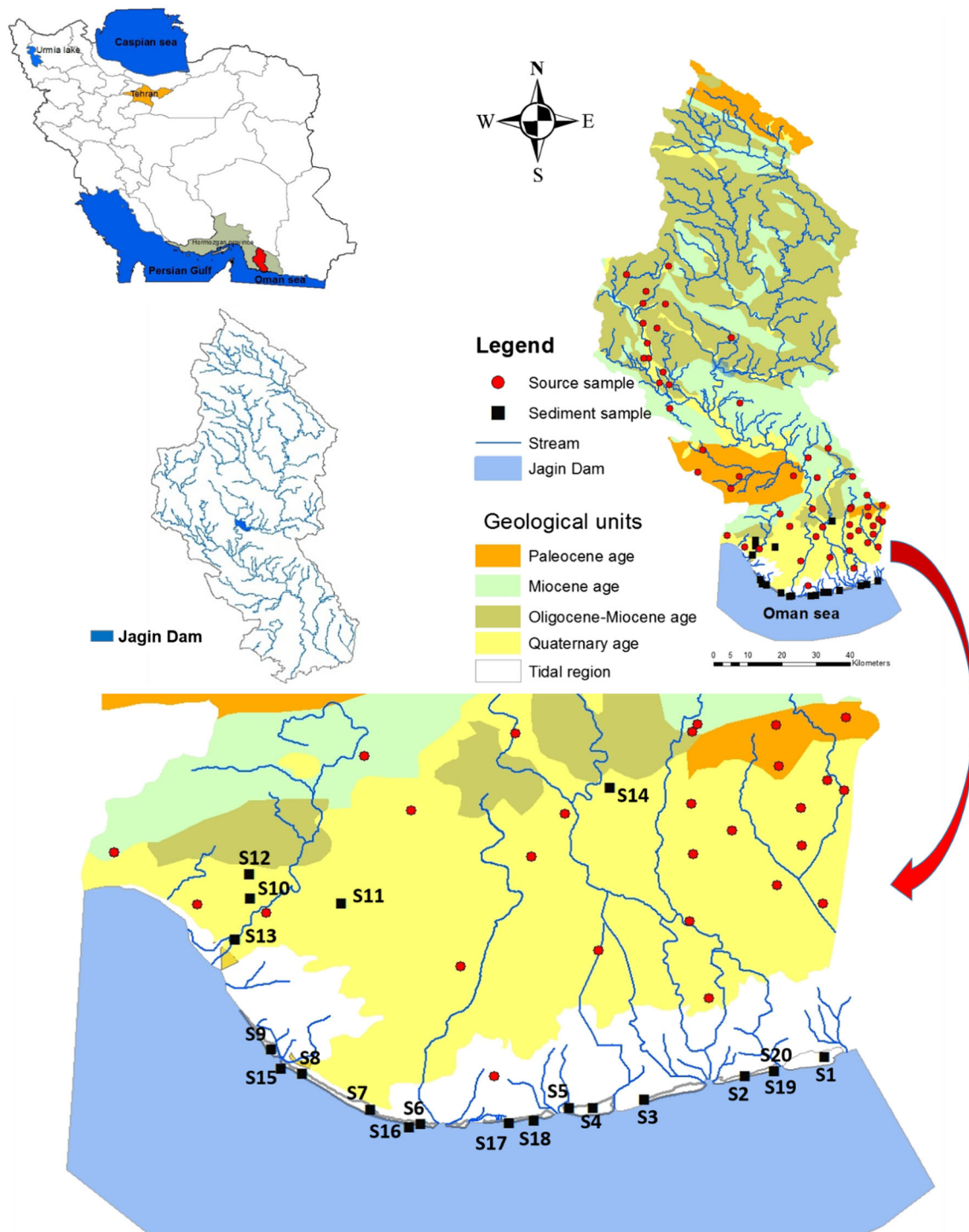


Fig. 1 Location of the Jagin study catchment in the Hormozgan province, southern Iran; geology, stream network, terrestrial source and target sediment sampling sites are shown

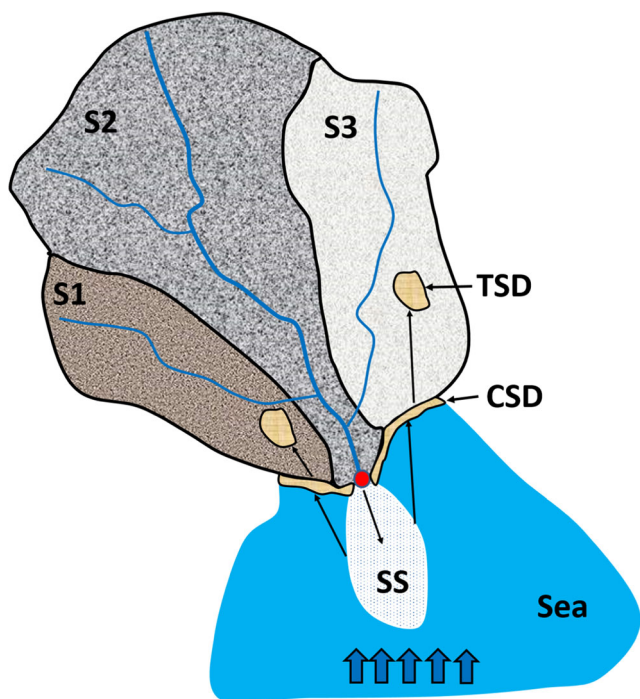


Fig. 2 Schematic of sediment transfer pathways from terrestrial sources to coastal sediment deposits. S1–S3, SS, TSD and CSD indicate terrestrial sediment sources, suspended sediment, terrestrial sand dunes and coastal sand dunes, respectively. The red circle marks the outlet of the study catchment. Blue arrows indicate the predominant direction of sea waves. TSD comprise material mobilized both fluvially and by wind from upstream which is then deposited and prone to subsequent wind erosion

(Pham et al. 2018); synthesis of grain-size, clay mineralogy, geochemistry and mineral magnetism (Prizomwala et al. 2014); geochemical properties (Rao et al. 2015; Saitoh et al. 2017), Nd-Sr isotopic ratios (Rosenbauer et al. 2013); rare earth elements (REE) (Rao et al. 2017); and optically

stimulated luminescence (OSL) and thermoluminescence (TL) (Zular et al. 2015). Whilst most of the studies listed above have been successful at inferring the critical sources of coastal sediment deposits prone to aeolian erosion, we note that, in many cases, quantitative sediment fingerprinting within an explicit uncertainty framework has not been used to ascribe coastal sediment provenance.

Sediment fingerprinting is a technique with increasing adoption rates (Walling 2013; Collins et al. 2017; Owens et al. 2016) which provides a basis for quantifying the contributions of discrete sources to different types of target sediment samples. To date, the approach has been most widely used to identify fluvial sediment sources in river catchments in different hydro-climatic settings (Collins et al. 1997, 2012; Walling et al. 1999; Russell et al. 2001; Mukundan et al. 2012; Haddadchi et al. 2013; Franz et al. 2014; Pulley and Collins 2018; Le Gall et al. 2016; Tiecher et al. 2018; Koiter et al. 2013; Zhang et al. 2017). Its application in aeolian geomorphology has emerged much more recently (Liu et al. 2016a; Gholami et al. 2017a, 2017b; Wang et al. 2017; Dahmardeh Behrooz et al. 2019), but there remains scope to continue testing the applicability of different tracers for discriminating and apportioning the contributions of critical sources to those coastal sediment deposits, within an uncertainty framework. In brief, sediment fingerprinting involves collecting target sediment samples and comparing their measured tracer properties with those of potential sediment sources. To date, a diverse range of tracer properties has been used by sediment fingerprinting studies including geochemistry (such as heavy metals, trace or rare earth elements; Collins and Walling 2007; Collins et al. 2010; Cashman et al. 2018; Tiecher et al. 2018), biomarkers (Chen et al. 2016), stable isotopes (Le Gall et al. 2016), fallout radionuclides (Wilkinson et al. 2013; Evrard et al. 2016), soil enzymes (Nosrati et al. 2011), colour

Fig. 3 Google Earth image showing the Jagin River transporting a high suspended sediment load during a flood in July 2004 and location of the sediment deposits included in the sampling strategy: MS, CD and TSD

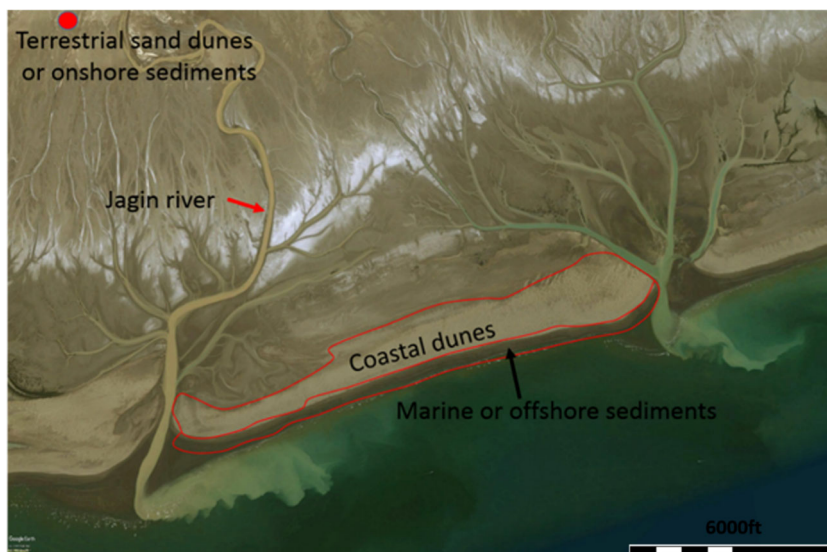


Table 1 Minimum and maximum concentrations of the geochemical tracers in the fine-grained (< 63 μm) fraction of source and target sediment samples

Tracer	Source		Sediment		Bracket test
	Min	Max	Min	Max	
Al	3.6	7.2	4.2	5.8	Passed
Ba	147	385	164	2482	Failed
Be	0.36	1.3	0.5	0.88	Passed
Ca	5.1	10.5	6.2	8.9	Passed
Ce	26.4	68.3	34	130	Failed
Co	11	32	11.7	27.5	Passed
Cr	55	191	80	848	Failed
CS	7.2	19.6	9	46.1	Failed
Cu	0.0015	0.005	0.0017	0.0038	Passed
Dy	2.7	5.2	3.5	8	Failed
Er	1.46	3.15	1.6	5	Failed
Eu	0.71	1.34	0.85	4.5	Failed
Fe	2.35	4.86	3.2	12.4	Failed
Ga	11	25	11.3	59.5	Failed
Gd	2	4.25	2.8	10.6	Failed
Hf	0.01	0.37	0.1	0.29	Passed
Ho	0.69	1.13	0.8	1.67	Failed
Zr	34.4	72.3	43.3	163	Failed
La	15.2	37.6	19.8	62.3	Failed
K	0.69	2.4	1.06	1.8	Passed
Li	9.4	45.5	16	35.2	Passed
Lu	0.14	0.28	0.18	0.78	Failed
Mg	1.1	3.7	1.32	3	Passed
Mn	558	997	716.9	1825	Failed
Mo	2.7	21	2.6	7	Failed
Na	1.15	3.74	1.52	3.8	Failed
Nb	5.5	12	6.9	42	Failed
Nd	29.3	63	36.2	59.3	Passed
Ni	50.4	147.6	59	133	Passed
P	0.04	0.09	0.05	0.1	Failed
Pb	4.1	61.1	9.9	29.6	Passed
Pr	1	6.8	3.4	17	Failed
Rb	33	105.3	29.65	65.8	Failed
Sc	6.6	16.4	9.1	20	Failed
Sm	2.9	6.2	3.34	10.5	Failed
Sn	4.4	21.6	7.5	102.7	Failed
Sr	164	2400	204.1	353.7	Passed
Tb	0.18	0.7	0.29	1.4	Failed
Te	0.11	0.8	0.13	0.47	Passed
Th	5.8	15.5	6.3	34.5	Failed
Ti	0.26	0.58	0.3	1.72	Failed
Tm	0.13	0.34	0.16	0.75	Failed
U	2.7	4.7	3.3	9.5	Failed
V	58	132	77.8	485	Failed
W	1.24	9.8	1.5	5.9	Passed
Y	12.8	23	15	34	Failed

Table 1 (continued)

Tracer	Source		Sediment		Bracket test
	Min	Max	Min	Max	
Yb	1.2	2.3	1.5	3.7	Failed
Zn	37	80	38	111	Failed

(Martínez-Carreras et al. 2010), grain size (Weltje 2012) and mineralogy (Walden et al. 1997). In some instances, a mix of different types of tracers has been used including, for example, a combination of grain size, soil organic matter (SOM) content, total nitrogen, phosphorus and potassium, magnetic susceptibility and geochemical elements (Zhang et al. 2017). Recent reviews are provided by Collins et al. (2017) and Owens et al. (2016).

Against the above background, the objective of this study was to quantify, using an explicit uncertainty framework, the relative contributions of terrestrial sources of dust prone to aeolian erosion to both fine- (< 63 μm) and coarse-grained (63–500 μm) sediments in three categories of coastal sediment deposits in the Jagin catchment, east of Jask, Hormozgan province, southern Iran, namely, coastal dunes (CD), terrestrial sand dunes (TSD) or onshore sediments and marine or offshore sediments (MS). In doing so, the study aimed to test the applicability of geochemical tracers for source discrimination and apportionment and thereby to report limitations and uncertainties to the user community.

Materials and methods

Study area

The Jagin catchment (25° 32'–26° 56' N and 57° 32'–58° 24' E) is located in the east of Jask, Hormozgan province, southern Iran and covers an area of 7340 km² (Fig. 1). The study area is located in a region where erosions by water and wind are serious threats in the upstream and downstream parts of catchments, respectively. Geologically, the Jagin catchment is underlain by deposits of four geological ages consisting of clay flat, high and low level fans and valley terraces (Quaternary age deposits); shale, gypsiferous mudstone and silty shale with minor mudstone and limestone (Sabz and Ghasr Gand geological units; Oligocene–Miocene age deposits); sandstone, siltstone, conglomerate, shale, mudstone and shell beds (Darpahn and Jagin geological units; Miocene age deposits); and sandstone with siltstone, mudstone and minor conglomerate (Palaeocene age deposits) (Fig. 1). Based on the Jask meteorological station, mean annual air temperatures range between 19 and 35.5 °C. Mean annual rainfall is ~ 162 mm. Based on the land use

Table 2 Minimum and maximum concentrations of the geochemical tracers in the coarse-grained (63–500 μm) fraction of source and target sediment samples

Tracer	Source		Sediment		Bracket test
	Min	Max	Min	Max	
Al	3.3	7.4	4	5.5	Passed
Ba	136	639	165	385	Passed
Be	0.29	1.3	0.52	0.9	Passed
Ca	4.6	11.7	7.2	14	Failed
Ce	22.3	39	26	33	Passed
Co	7.5	30.3	7.2	16	Failed
Cr	40.1	159	46	81	Passed
CS	4.7	18.6	2.3	8.6	Failed
Cu	0.001	0.0053	0.0012	0.0025	Passed
Dy	2.3	4.4	3	3.6	Passed
Er	1.26	2.8	1.4	1.72	Passed
Eu	0.6	1	0.7	0.9	Passed
Fe	1.8	5	2	3.2	Passed
Ga	7.4	16.3	7.5	11.4	Passed
Gd	1.7	3.9	1.8	2.8	Passed
Hf	0	0.3	0.04	0.11	Passed
Ho	0.67	0.95	0.7	0.82	Passed
Zr	27	62.5	28	43.3	Passed
La	16.5	27	18	22	Passed
K	0.63	2.44	1	1.7	Passed
Li	9.4	45	11.4	31	Passed
Lu	0.1	0.29	0.11	0.19	Passed
Mg	0.9	3.1	1	2.7	Passed
Mn	513	1012	696	1194	Failed
Mo	2.6	18.4	2.1	5.2	Failed
Na	1	7.5	1.7	3.6	Passed
Nb	2.7	12	3.9	6.9	Passed
Nd	31.2	61	37	63.2	Failed
Ni	32	161	40	74.5	Passed
P	0.01	0.08	0.03	0.09	Failed
Pb	4.6	73	5.6	13	Passed
Pr	0.8	7.3	2.9	5.9	Passed
Rb	27	102.5	28.9	69	Passed
Sc	5.9	17	7	10.2	Passed
Sm	2.2	4.5	2.3	3.4	Passed
Sn	1.1	20	3.74	9.4	Passed
Sr	149	611	214	595	Failed
Tb	0.1	0.59	0.14	0.48	Passed
Te	0.1	0.72	0.08	0.15	Passed
Th	3.6	14.2	3.7	7.1	Passed
Ti	0.21	0.39	0.2	0.29	Passed
Tm	0.08	0.31	0.1	0.17	Passed
U	2.4	4.3	2.6	3.3	Passed
V	45	133	48	79	Passed
W	0.62	9	1	5.6	Passed
Y	12	17.4	12.6	14.5	Passed

Table 2 (continued)

Tracer	Source		Sediment		Bracket test
	Min	Max	Min	Max	
Yb	1	1.8	1.2	1.4	Passed
Zn	25	79	27	52	Passed

map of Iran provided by IFRWMO, the land use of the study area includes rangelands (53%), rock outcrops (27%), bare land (14%), salt lands (5%), planting for combating wind erosion and for stabilizing sand dunes (0.6%), orchards (0.08%), agricultural land (0.06%) and mangrove forests (0.01%).

The approach

The fingerprinting approach (shown schematically in Fig. 2) adopted in this study involved the comparison of target sediment samples collected from three categories of coastal sediment deposits (CD, TSD and MS) with terrestrial source samples used to characterize different geological units. The study focused on terrestrial sources of aeolian dust in coastal deposits since these were judged to be more important than alternative sources.

Sampling and laboratory work

Source samples were collected from the surficial layer (0–2 cm) of four geological spatial sources consisting of Quaternary (Q) ($n = 32$), Palaeocene (P) ($n = 8$), Miocene (M) ($n = 12$) and Oligocene–Miocene (OM) ($n = 10$) age deposits (Fig. 1). Twenty target sediment samples were taken from three different positions comprising nine coastal dune samples (CD; S1–S9), five terrestrial sand dune or onshore samples (TSD; S10–S14) and six marine sediment or offshore samples (MS; S15–S20) (Figs. 1 and 3). All sediment and source samples were air-dried and dry sieved using $< 63 \mu\text{m}$ (fine-grained fraction) and $63\text{--}500 \mu\text{m}$ (coarse-grained fraction) meshes. The geochemical analysis of the sediment and source samples was carried out after acid digestion with aqua regia (Collins et al. 2012). Forty-nine geochemical elements including Al, Ba, Be, Ca, Ce, Co, Cr, Cs, Cu, Dy, Er, Eu, Fe, Ga, Gd, Hf, Ho, In, La, K, Li, Lu, Mg, Mn, Mo, Na, Nb, Nd, Ni, P, Pb, Pr, Rb, Sc, Sm, Sn, Sr, Tb, Te, Th, Ti, Tm, U, V, W, Y, Yb, Zn and Zr were measured at the fine-grained and coarse-grained fractions ($< 63 \mu\text{m}$ and $63\text{--}500 \mu\text{m}$) using ICP-OES in the central laboratory of University of Hormozgan, Iran.

Selection of final composite fingerprints for terrestrial source discrimination

Prior to applying a statistical procedure for selecting final fingerprints, a range or so-called bracket test (Collins et al. 2010; Gellis and Noe 2013) was used to identify outliers and, therefore, significantly non-conservative tracers for exclusion from further analysis. Here, the maximum and minimum tracer concentrations in the source and sediment samples were used for identifying outliers. Tracers failing the bracket test (i.e. tracer concentrations measured for the target sediment samples fell outside the corresponding ranges of the source sample tracer concentrations) were removed from further analysis (Nosrati et al. 2018). In step 2, a two-stage statistical process (Collins et al. 1997) was applied to select final composite fingerprints for source discrimination. In step 1, the Kruskal–Wallis H test was used to assess the ability of individual properties for discriminating the three sources. All properties passing the Kruskal–Wallis H test entered stage 2. In this second stage, stepwise discriminant function analysis (DFA) based on the minimization of Wilks' lambda was used to identify the final signatures for tracing the sources of both the < 63 μm and 63–500 μm size fractions of the target sediment samples. As a further test of tracer conservation, bi-plots of all tracers comprising the final composite signatures were used to assess similarities in the relationships between tracers in source and target sediment samples.

Terrestrial source apportionment using a Monte Carlo simulation framework

Results produced by sediment fingerprinting studies have various inherent uncertainties (Walling 2013).

Two principal data processing frameworks are widely used to quantify the uncertainties associated with sediment fingerprinting results. Many studies (e.g., Franks and Rowan 2000; Collins et al. 2013a, b, 2014; Stone et al. 2014; Liu et al. 2016b; Pulley and Collins 2018; Habibi et al. 2019) have used a frequentist approach incorporating a Monte Carlo framework for uncertainty analysis. Alternatively, Bayesian approaches have also been used to evaluate uncertainties associated with the results generated by sediment fingerprinting (Nosrati et al. 2018; Gholami et al. 2017b; Cooper et al. 2014, 2015; Abban et al. 2016; Cooper and Krueger 2017; Habibi et al. 2019). Here, a critical factor influencing the choice of data processing framework concerns whether the source and sediment tracer data satisfy the requirements of Bayesian methods, including exhibiting normal distributions. In many instances, tracer data do not satisfy this basic requirement (Collins et al. 2013a, b, 2014).

We used a Monte Carlo simulation framework, proposed by Collins et al. (2012), to determine the contributions of the terrestrial sources to the target coastal sediment sample and the corresponding uncertainty ranges for those contributions. In reality, only a limited number of source and target sediment samples can be collected by any fingerprinting investigation (Collins et al. 2017). This limitation results in uncertainty in the estimation of sediment source contributions. One means of taking explicit account of the uncertainties generated by limited sample numbers involves the use of a Monte Carlo simulation framework in conjunction with the un-mixing model (Eq. 1) used to apportion sediment sources. Here, the means and standard deviations of the tracer data for the source and target

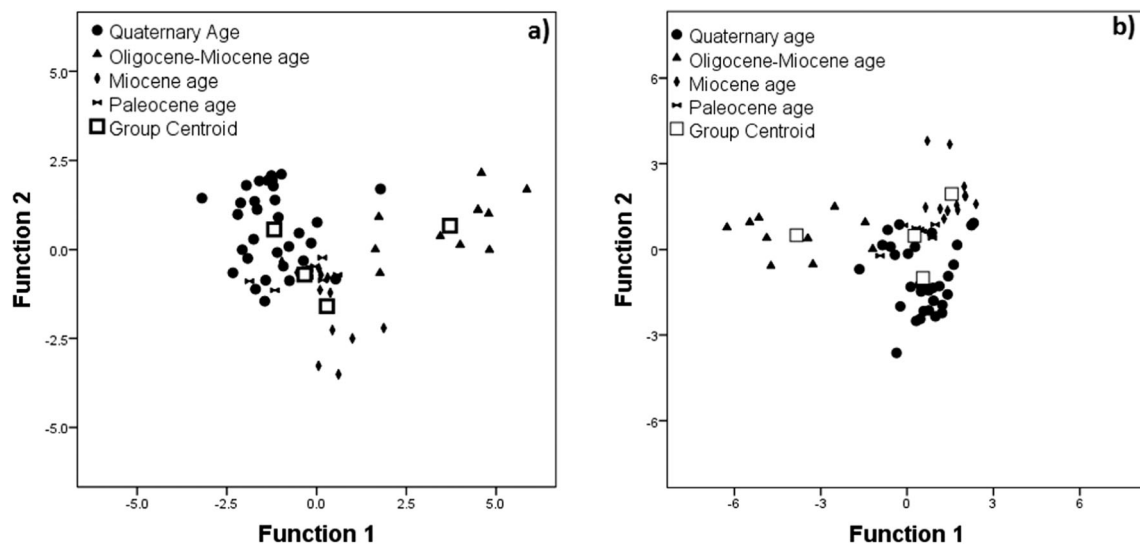


Fig. 4 Scatter plots of the first and second discriminant functions derived from stepwise DFA. **a** Fine-grained fraction. **b** Coarse-grained fraction

Table 3 The results of the Kruskal–Wallis H test and stepwise DFA for the ability of the individual geochemical tracers and final composite fingerprints to discriminate the source samples, using either the fine- or

coarse-grained fractions, respectively. *Statistically significant at $p \leq 0.05$; **statistically significant at $p \leq 0.01$; and ns not statistically significant at $p \leq 0.05$

Fine-grained fraction					Coarse-grained fraction				
Kruskal–Wallis H test			Stepwise DFA		Kruskal–Wallis H test			Stepwise DFA	
Tracer	H value	P value	Tracer selected	Wilks' lambda	Tracer	H value	P value	Tracer selected	Wilks' lambda
Al	17.46	0.001**	Be	0.459	Al	14.72	0.002**	Cu	0.431
Be	26.37	0.000**	Ni	0.257	Ba	3.34	0.342ns	Th	0.246
Ca	19.35	0.000**	K	0.171	Be	18.48	0.000**	Be	0.158
Co	16.43	0.001**	Cu	0.128	Ce	4.9	0.179ns	Al	0.118
Cu	21.48	0.000**			Cr	17.44	0.001**	La	0.096
Hf	5.15	0.16ns			Cu	24.23	0.000**	Mg	0.078
K	21	0.000**			Dy	17.47	0.001**	Fe	0.063
Li	21.02	0.000**			Er	14.68	0.002**		
Mg	9.7	0.021*			Eu	10.31	0.016*		
Nd	22.01	0.000**			Fe	23.7	0.000**		
Ni	12.81	0.005**			Ga	18.5	0.000**		
Pb	5.89	0.117ns			Gd	23.54	0.000**		
Sr	11.4	0.01*			Hf	1.62	0.654ns		
Te	11.24	0.01*			Ho	2.59	0.485ns		
W	7.18	0.066ns			La	21.41	0.000**		
					K	12.58	0.005**		
					Li	17.22	0.001**		
					Lu	22.23	0.000**		
					Mg	15.85	0.001**		
					Na	20.82	0.000**		
					Nb	19.98	0.000**		
					Ni	19.56	0.000**		
					Pb	14.08	0.003**		
					Pr	28.01	0.000**		
					Rb	8.81	0.032*		
					Sc	20.19	0.000**		
					Sm	13.14	0.004**		
					Sn	13.06	0.005**		
					Sr	6.45	0.092ns		
					Tb	11.56	0.009**		
					Th	19.93	0.000**		
					Tm	17.74	0.000**		
					U	22.28	0.000**		
					V	24.33	0.000**		
					W	7.69	0.053ns		
					Y	8.8	0.032*		
					Yb	5.86	0.118ns		
					Zn	20.02	0.000**		
					Zr	12.81	0.005**		

sediment samples are used to construct probability density distributions (pdfs; Hughes et al. 2009; Collins

et al. 2013a, b; Brosinsky et al. 2014) and these are repeat sampled during the Monte Carlo simulations to

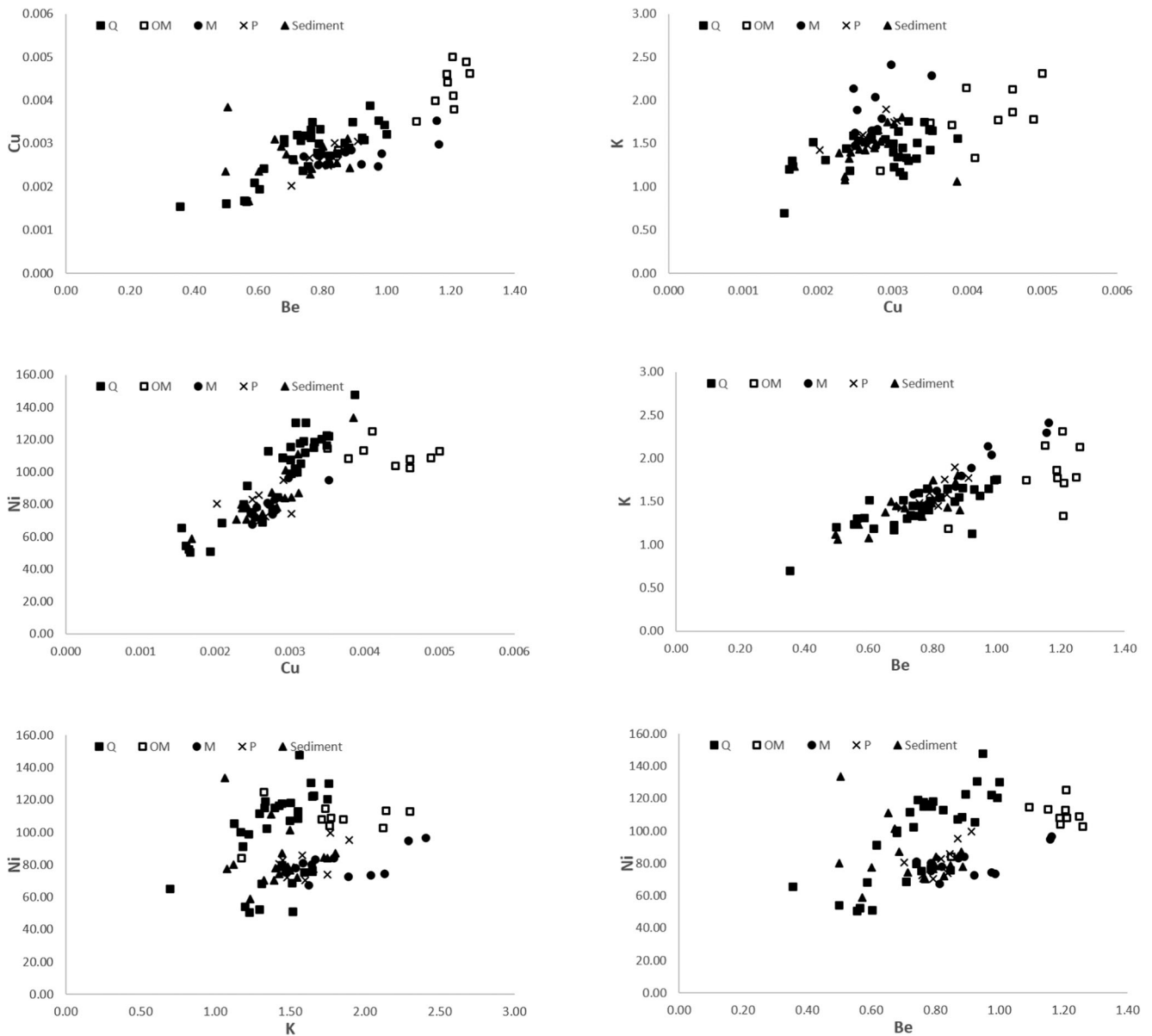


Fig. 5 Bi-plots for all pairings of the geochemical tracers in the final composite signature, measured on the fine-grained (< 63 μm) fraction of the source and target sediment samples. Q, P, M and OM indicate

Quaternary, Palaeocene, Miocene and Oligocene–Miocene age deposits, respectively

generate deviate source and target sediment sample mean tracer values for estimating source proportions (Hughes et al. 2009; Voli et al. 2013; Collins et al. 2013a, b; Brosinsky et al. 2014). Using Latin hypercube sampling (LHS), 10,000 random samples were drawn from the pdfs to permit Eq. 1 to be solved 10,000 times. Proportional source estimates generated by the Monte Carlo simulations were, in turn, converted to pdfs and used to provide 95% confidence intervals for source contributions based on the 2.5 and 97.5 percentiles of the predicted source contributions for each target sediment sample. The structure of the un-mixing model is provided by the following

objective function ($f(X_j)$) which is minimized during the Monte Carlo routine (Collins et al. 1997):

$$f(X_j) = \sum_{i=1}^n \left(\left(C_i - \sum_{j=1}^m P_j \cdot X_{j,i} \right) / C_i \right)^2 \tag{1}$$

where n is the number of fingerprint properties, m is the number of sediment sources, C_i is the deviate mean concentration of fingerprint property (i) in the target sediment sample, P_j is the deviate relative contribution of source (j) to the target sediment sample and $X_{j,i}$ is the deviate mean concentration

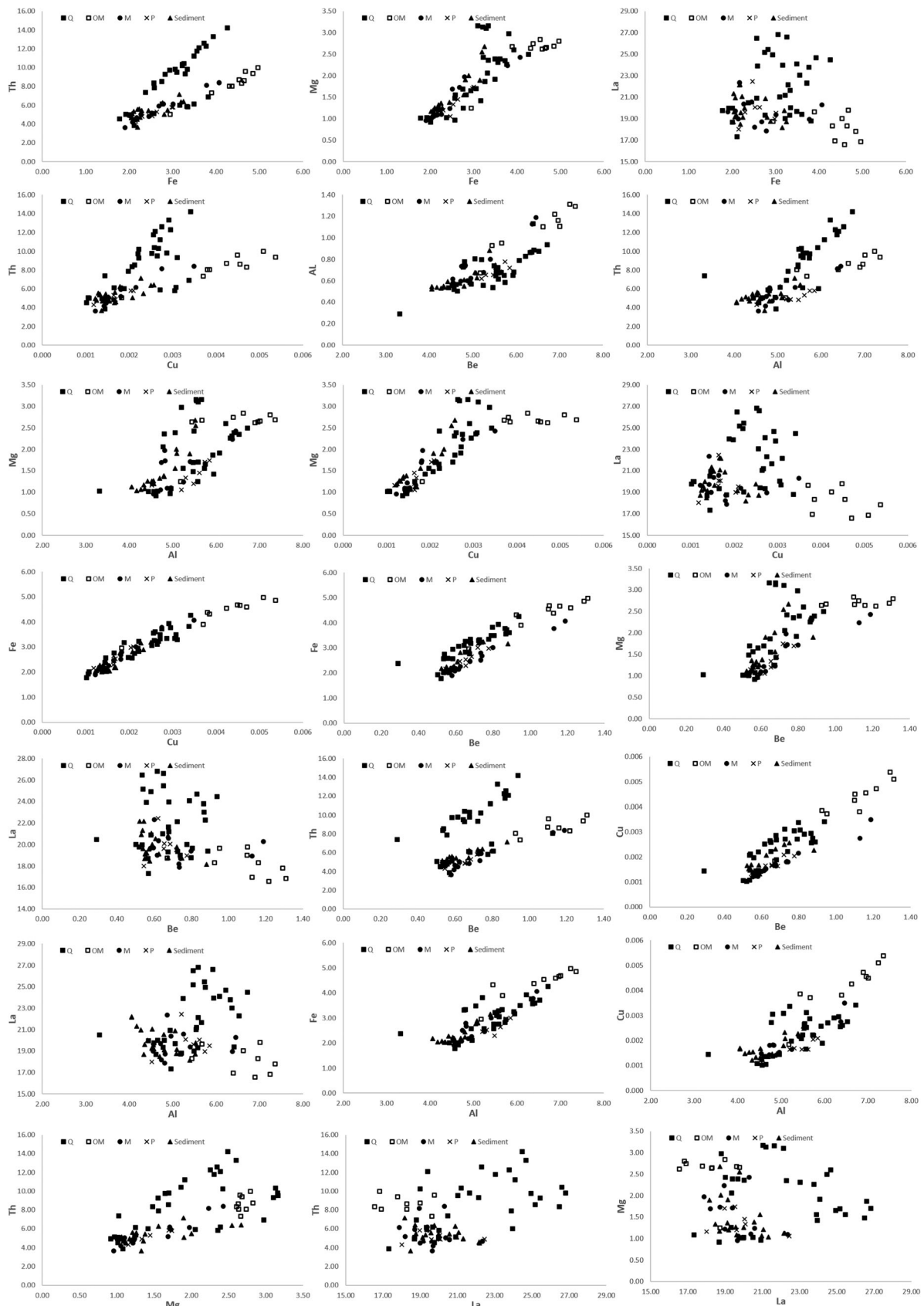


Fig. 6 Bi-plots for all pairings of the geochemical tracers in the final composite signature, measured on the coarse-grained (63–500 μm) fraction of the source and target sediment samples. Q, P, M and OM indicate Quaternary, Palaeocene, Miocene and Oligocene–Miocene age deposits, respectively

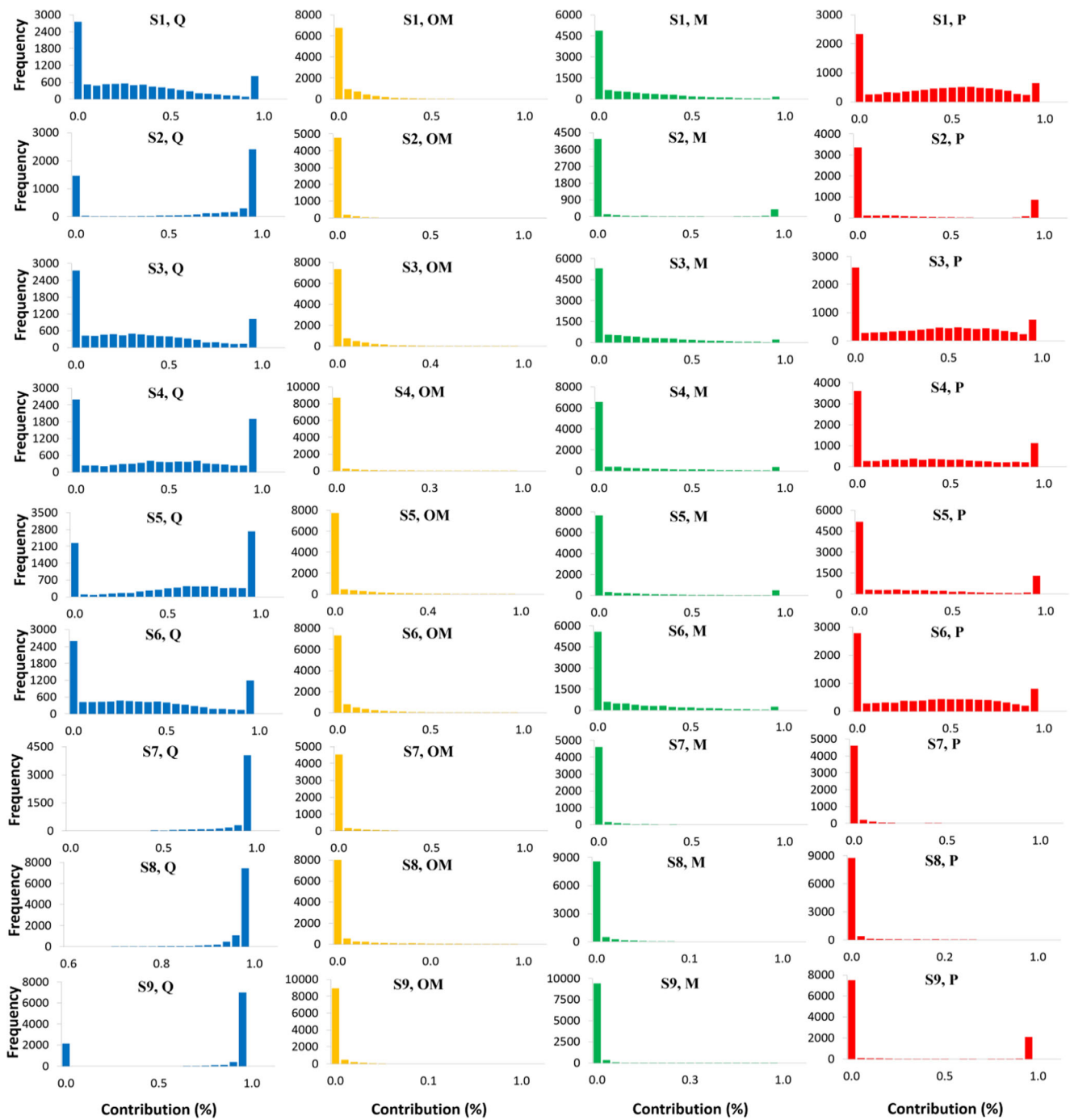


Fig. 7 Probability density functions of the Monte Carlo simulation results for estimating the sources of fine-grained sediment in CD samples (S1–S9)

of fingerprint property (*i*) in source (*j*). The multivariate un-mixing model must satisfy two boundary constraints:

$$0 \leq P_j \leq 1 \tag{2}$$

$$\sum P_j = 1 \tag{3}$$

The goodness-of-fit (GOF) suggested by Manjoro et al. (2016) was used to evaluate un-mixing model performance in

terms of the fit between the source-weighted predicted and measured tracer concentrations for the target sediment samples, viz.:

$$GOF = \left(1 - \left[\text{SQRT}^{\sum_{i=1}^n \left\{ \left(C_i - \left(\sum_{j=1}^m P_j \cdot X_{ji} \right) \right) / C_i \right\}^2} \right] \right) / n \tag{4}$$

The accuracy of the modelled estimates of terrestrial source proportions was evaluated using a virtual, rather

Table 4 The average mean contributions from the geological spatial sources to the fine-grained fraction in the three categories of coastal sediment deposits comprising: CD, TSD and MD

Sediment category	Sediment sample no.	Geological spatial source			
		Q	OM	M	P
CD	S1	33	6	18	43
	S2	26	1	13	60
	S3	36	5	17	42
	S4	47	3	14	36
	S5	58	5	10	27
	S6	38	5	16	41
	S7	100	0	0	0
	S8	98	0	0	2
	S9	77	0	1	22
Contribution (%)		57	3	10	30
TSD	S10	48	4	15	33
	S11	50	2	15	33
	S12	44	5	15	36
	S13	58	2	13	27
	S14	29	4	21	46
Contribution (%)		46	3	16	35
MD	S15	15	18	29	38
	S16	15	15	32	38
	S17	11	24	34	31
	S18	20	6	27	47
	S19	47	4	13	36
	S20	45	6	13	36
Contribution (%)		25	12	25	38

than artificial, mixture test (Haddadchi et al. 2014; Pulley and Collins 2018). Here, the un-mixing model was evaluated against the known source proportions comprising six artificial sediment mixtures. The outcomes of the virtual mixtures tests were assessed using root mean squared error (RMSE) and mean absolute error (MAE), viz.:

$$\text{RMSE} = \sqrt{\frac{\sum_{i=1}^n (Y_{\text{Known}} - Y_{\text{Predicted}})^2}{n}} \quad (5)$$

$$\left(\text{MAE} = \frac{\sum_{i=1}^n |Y_{\text{Known}} - Y_{\text{Predicted}}|}{n} \right) \quad (6)$$

where Y_{Known} is known percentage source contribution in the artificial mixture, $Y_{\text{Predicted}}$ is percentage source contribution predicted by the model and n represents the number of sediment sources ($n = 3$).

Results and discussion

Terrestrial sediment source discrimination

Step 1: range or bracket test

For the fine-grained fraction, 33 properties (Ba, Ce, Cr, Cs, Dy, Er, Eu, Fe, Ga, Gd, Ho, In, La, Lu, Mn, Mo, Na, Nb, P, Pr, Rb, Sc, Sm, Sn, Tb, Th, Ti, Tm, U, V, Y, Yb, Zn and Zr) were identified as outliers (Table 1). For the coarse-grained fraction, concentrations of nine properties (Ca, Co, Cs, Mn, Mo, Nd, P, Te and Ti) measured in the target sediment samples were outside of their corresponding ranges in the source samples (Table 2). In both cases, these properties were assumed to be non-conservative for the two size fractions in the study area and thereby excluded from further analysis. Previous studies using geochemical properties as sediment source fingerprints, albeit in different environmental settings, have reported reasonably high failure rates on the basis of the range test (e.g., Gellis and Noe 2013; Collins et al. 2013a, b). Non-conservative behaviour is also typically greater in the finest fractions (Collins et al. 2017). Whilst failure of the bracket test might result from the absence of a source in the sampling strategy, this specific reason would most likely result in consistently high failure of the conservation test across both size fractions. Since that was not the case here, it is more likely that various biogeochemical processes are responsible for the non-conservative behaviour of the tracers in the fine-grained fraction.

Step 2: Kruskal–Wallis H test and stepwise DFA

All properties passing the range or bracket test were further assessed using the Kruskal–Wallis H test. For the fine-grained fraction, three tracers (Hf, Pb and W) of the 16 properties passing the range test failed the Kruskal–Wallis H test at $p < 0.05$ (Table 3). Among the 39 properties passing the bracket test for the coarse-grained fraction, seven properties (Ba, Ce, Hf, Ho, Sr, W and Yb) were not significantly different at $p \leq 0.05$. In both cases, all properties with $p \leq 0.05$ were used in the next step of statistical analysis for sediment source discrimination.

Based on the stepwise DFA, four (Be, Ni, K and Cu) and seven (Cu, Th, Be, Al, La, Mg and Fe) properties were identified in the final composite signatures for source discrimination using the fine- and coarse-grained fractions, respectively (Table 3). The results of the stepwise DFA (Table 3; Fig. 4) indicated that 74% and 85.5% of the source samples were classified correctly for the fine- and coarse-grained fractions, respectively using these final signatures. Previous studies have reported similarly low source sample discrimination rates albeit in different environmental situations (e.g. Owens et al. 1999; Bottrill et al. 2000).

Step 3: bi-plot tests for the tracers in the final composite fingerprints

Results from the bi-plot tests for the fine- and coarse-grained fractions are presented in Figs. 5 and 6, respectively. Plots wherein the source and sediment samples do not fall in the same general space suggest non-conservative behaviour of the tracers in question. Generally speaking, the plots in Figs. 5 and 6 suggested conservative behaviour for the tracers comprising the final composite signatures used to discriminate the two size fractions of the potential terrestrial sediment sources.

Terrestrial source apportionment—fine-grained sediment fraction

Figure 7 presents probability density functions (pdfs) for the Monte Carlo simulations for predicting the geological spatial sources of fine-grained sediments in CD samples (S1–S9). Corresponding average mean source proportions are presented in Table 4. The mean contribution from the Quaternary age terrestrial spatial source was estimated at 57% (corresponding uncertainty range; 0–100%). Mean contributions from the Oligocene–Miocene, Miocene and Palaeocene age terrestrial spatial sources were estimated at 3% (uncertainty range 0–100%), 10% (uncertainty range 0–100%) and 30% (uncertainty range 0–100%), respectively (Fig. 7; Table 4).

Figure 8 and Table 4 show the corresponding source apportionment results for the four geological spatial sources of fine-grained sediment in TSD (S10–S14). In this case, fine-grained sediment contributions from the Quaternary, Oligocene–Miocene, Miocene and Palaeocene age spatial sources were estimated 46% (uncertainty range 0–100%), 3% (uncertainty range 0–100%), 16% (uncertainty range 0–100%) and 35% (uncertainty range 0–100%), respectively (Fig. 8; Table 4).

The uncertainty ranges for the predicted source contributions to the fine-grained sediments in MD (S15–S20) are illustrated in Fig. 9. Corresponding average mean contributions are shown in Table 4. North Wyke Palaeocene age deposits were predicted to be the main spatial source (38%; uncertainty range 0–100%). The mean contributions from the Quaternary, Oligocene–Miocene and Miocene geological spatial sources were estimated at 25% (uncertainty range 0–100%), 12% (uncertainty range 0–100%) and 25% (uncertainty range 0–100%), respectively (Fig. 9; Table 4).

Terrestrial source apportionment—coarse-grained sediment fraction

Figure 10 presents the uncertainty ranges for the predicted contributions from the four geological spatial sources to the coarse-grained sediment fraction in CD samples (S1–S9).

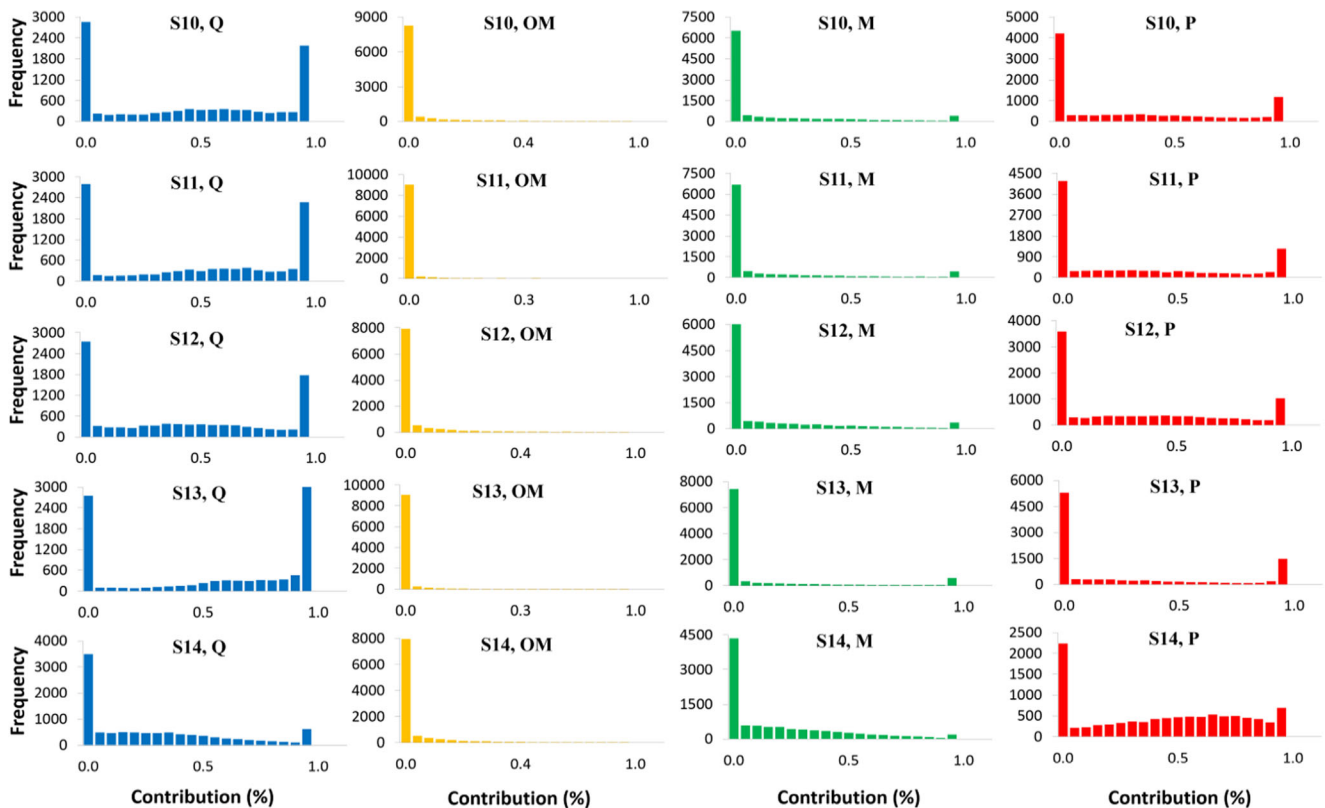


Fig. 8 Probability density functions of the Monte Carlo simulation results for estimating the sources of fine-grained sediment in TSD samples (S10–S14)

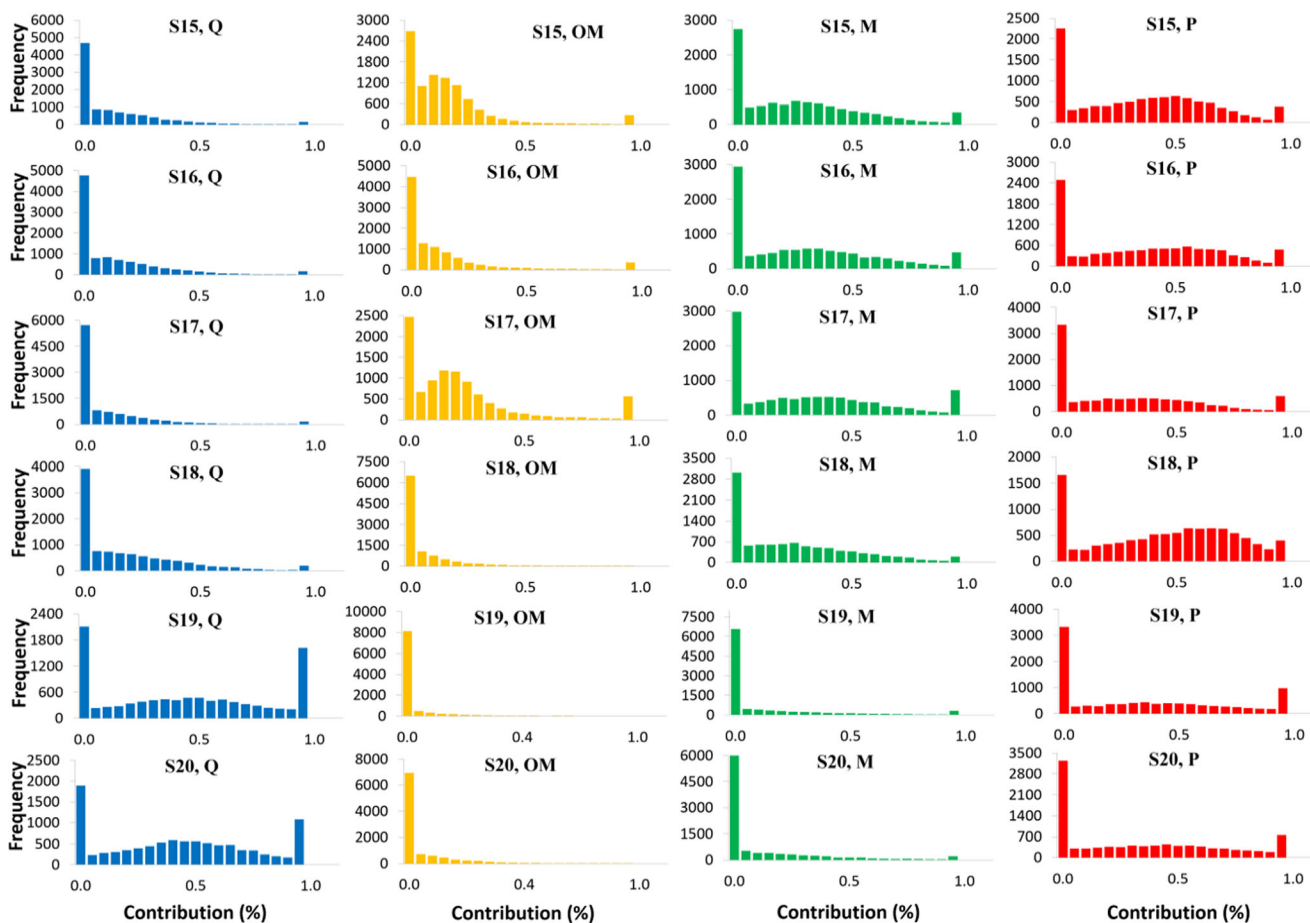


Fig. 9 Probability density functions of the Monte Carlo simulation results for estimating the sources of fine-grained sediment in MD samples (S15–S20)

Table 5 shows the corresponding average mean contributions from the individual terrestrial sources to the coarse-grained fraction. The predicted mean contributions from the Quaternary age deposits ranged between 0 and 100%, with a corresponding average mean contribution of 4%. The average mean contributions from the Oligocene–Miocene, Miocene and Palaeocene geological spatial sources were calculated at 0% (uncertainty range 0–100%), 17% (uncertainty range 0–100%) and 79% (uncertainty range 0–100%) (Fig. 10; Table 5).

The uncertainty ranges estimated for the spatial source contributions to coarse-grained sediment in TSD samples (S10–S14) are presented in Fig. 11. Ranges in the contributions from the Quaternary, Oligocene–Miocene, Miocene and Palaeocene age spatial sources were calculated as 0–100% (average mean contribution 9%), 0–100% (average mean contribution 8%), 0–100% (average mean contribution 20%) and 0–100% (average mean contribution 63%), respectively (Fig. 11; Table 5).

Figure 12 presents the estimated source contribution ranges for the coarse-grained fraction in MD samples (S15–S20). Here, the average mean contributions from the Quaternary, Oligocene–Miocene, Miocene and Palaeocene age spatial

sources were estimated 12% (uncertainty range 0–100%), 13% (uncertainty range 0–100%), 21% (uncertainty range 0–100%) and 54% (uncertainty range 0–100%), respectively (Fig. 11; Table 5).

Evaluation of the predicted terrestrial source proportions using virtual mixtures

The un-mixing model accuracy was tested using virtual sample mixtures of tracer values (Pulley and Collins 2018; Haddadchi et al. 2014). The comparison between predicted and known source proportions is presented in Table 6.

Table 7 shows the corresponding results of RMSE and MAE tests for evaluating the accuracy of the un-mixing model results for the fine- and coarse-grained fractions (S1–S6). For the fine-grained fraction (< 63 μm), the poorest performance on the basis of RMSE (11.1%) and MAE (3.8%) was estimated for S4, whereas the best performance (RMSE 2.3%, MAE 0.02%) was calculated for S6.

For the coarse-grained (63–500 μm) fraction, the best model performance using RMSE (1.7%) and MAE (0.2%) was estimated for S2, whereas the worst performance (RMSE 15.2%, MAE 4.7%) was calculated for S3.

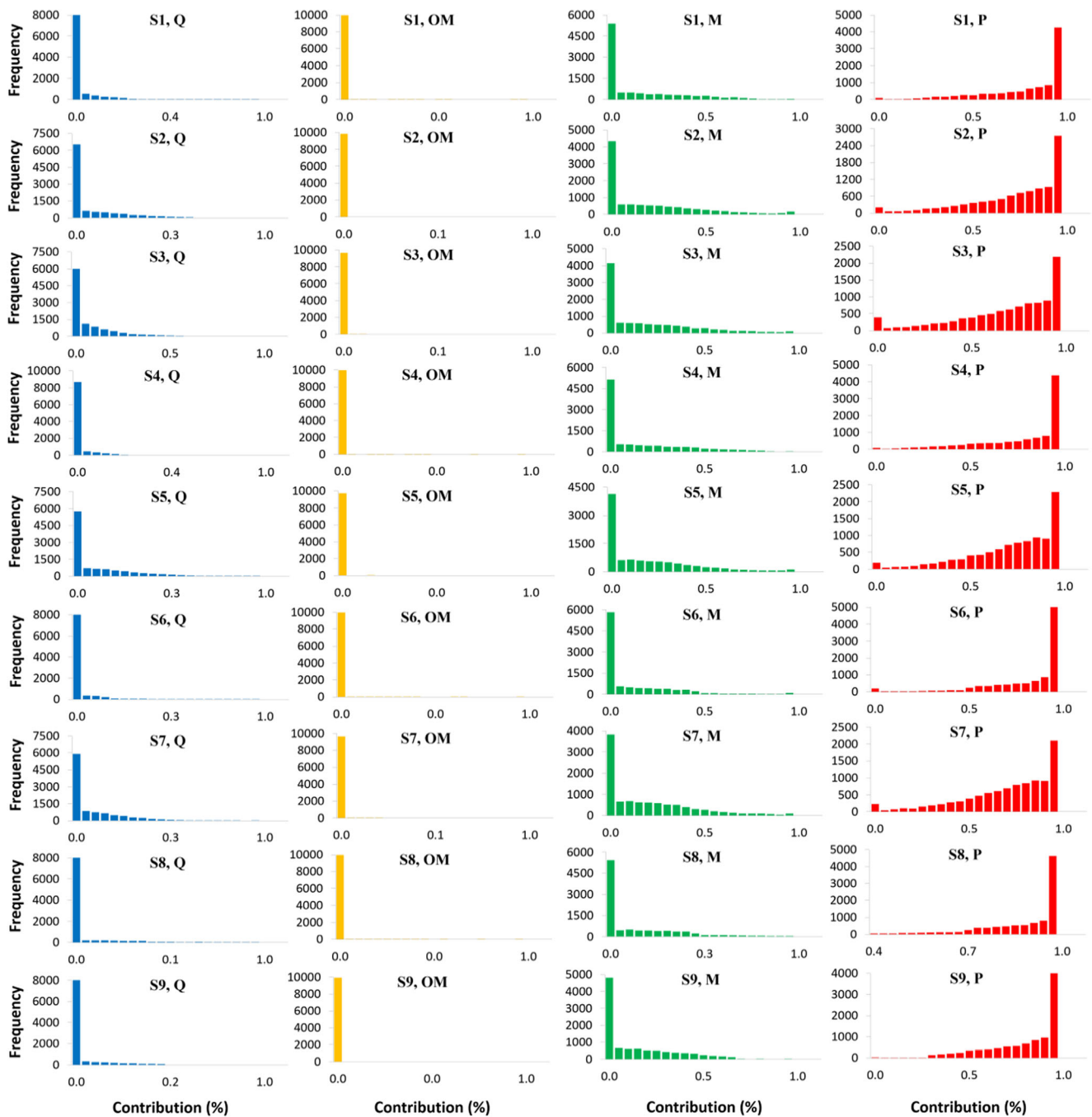


Fig. 10 Probability density functions of the Monte Carlo simulation results for estimating the sources of coarse-grained sediment in CD samples (S1–S9)

Based on the Monte Carlo modelling approach, the full uncertainty ranges (frequently 0–100%; Figs. 7, 8, 9, 10, 11 and 12) were estimated for the spatial source contributions to both fine-grained and coarse-grained sediments in the three categories of coastal deposits (CD, TSD and MD). These full uncertainty ranges for the predicted mean source proportions represent feasible solutions. Since these uncertainty ranges are based, in part, on the corresponding variation in source fingerprints, the latter should be considered carefully in the selection of tracers properties, in addition to mass conservation alone.

Overall, the source apportionment modelling suggested that the Quaternary (consisting of clay flats, alluvial fans and terraces) and Palaeocene (including sandstones, mudstones and minor conglomerate) age deposits are the main sources for fine-grained sediment samples collected from CD, TSD and MD deposits. The Palaeocene age deposits (including sandstones, mudstones and minor conglomerate) were identified as the main source of the coarse-grained sediment samples collected from the CD, TSD and MD deposits.

Table 5 The average mean contributions from the geological spatial sources to the coarse-grained fraction in the three categories of coastal sediment deposits comprising: CD, TSD and MD

Sediment category	Sediment sample no	Geological spatial source			
		Q	OM	M	P
CD	S1	3	0	16	81
	S2	4	0	20	76
	S3	8	0	21	71
	S4	2	0	17	81
	S5	6	0	20	74
	S6	2	0	13	85
	S7	6	0	21	73
	S8	1	0	10	89
	S9	1	0	16	83
Contribution (%)		4	0	17	79
TSD	S10	14	33	24	29
	S11	8	1	20	71
	S12	17	6	20	57
	S13	2	0	20	78
	S14	2	0	16	82
Contribution (%)		9	8	20	63
MD	S15	20	33	21	26
	S16	12	6	23	59
	S17	21	28	21	30
	S18	14	12	24	50
	S19	1	0	16	83
	S20	4	0	19	77
Contribution (%)		12	13	21	54

The above apportionment results suggest that the fine-grained (< 63 μm) fraction of coastal sediments mainly originates from the clay flats located in the lowlands in the vicinity of the study catchment outlet. Different landforms exhibit varying potentials such as dust sources due to the limitations on emissions imposed by differences in the supply of fine sediment and subsequent availability of this sediment for entrainment (Muhs et al. 2014). Rao et al. (2011) suggested a provenance local to the sampled deposits (< 75 μm fraction), with the source in that case being fluvial materials in the Yellow River.

The source apportionment results reported herein suggested that the coarse-grained (63–500 μm) fraction of the samples collected from the three categories of coastal sediment deposits mainly originates from sandstone and conglomerate sources located in the upstream mountains. In contrast, Du et al. (2018) reported that the coarse-grained fraction of sand dunes sampled in the Qaidam Basin, Tibetan Plateau, has a local origin comprising fluvial and alluvial sediments. Similarly, Gholami et al. (2017b) reported that Quaternary alluvial fans and terraces (alluvial sediments) are

the main source of the coarse-grained (62.5–150 μm) fraction of samples collected from the sand dunes in the Yazd-Ardekan plain in Central Iran. Ahmady-Birgani et al. (2018) reported that samples retrieved from the Urmia Lake sand dunes, north-western Iran, originated from alluvial and fluvial processes, with wind erosion acting as a secondary agent but playing an important role in the source contributions to the sediment deposited in the lower reaches of the study area.

Limitations of the fingerprinting approach for estimating sediment provenance

A principal limitation for source analysis of sediments at large-scale concerns the uncertainty associated with the collection of a limited number of source and sediment deposit samples. Where resources permit, high-density sampling is preferable (Wang et al. 2017). In the study area, however, there were limitations related to complex topography and the remoteness and extensive area of the Jagin study catchment. The uncertainty resulting from the sampling programme was assessed explicitly using a Monte Carlo framework, but interpretation of the results should, nevertheless, bear in mind the sampling density. The latter continues to represent an important challenge for all source tracing investigations using sediment fingerprinting. Although tracer conservation was assessed using a bracket test and bi-plots of tracer pairings in the two grain size fractions of the source and sediment samples, these procedures do not confirm the complete absence of any transformation. The study did not undertake any work to investigate the potential reasons for non-conservative behaviour which might include biogeochemical alterations arising from sorption, dissolution, precipitation, reduction or oxidation. The lack of such work continues to be common to the vast majority of source fingerprinting investigations, and this gap thereby requires further attention. Tracer conservation could be tested using both laboratory pot-scale experiments in controlled surroundings simulating local ambient environmental conditions (e.g. temperature, sunlight, rainfall) and plot-scale experiments to examine the likelihood of non-conservative behaviour over short transport distances. Here, however, the construction of pdfs for the sediment sample tracer values in each size fraction, and the Latin hypercube driven sampling of those pdfs, means that ranges in the sediment tracer values were used explicitly and those ranges are likely to help represent the likely impacts of any tracer transformation. Source apportionment estimates commonly differ on the basis of using composite signatures comprising different types of tracers. As a result, the interpretation of the source apportionment estimates generated by this study should bear in mind that final composite signatures were only constructed using geochemical tracers rather than multiple tracer types. The high failure rate, returned for the range test using the fine-grained fraction, suggests that geochemical tracers should

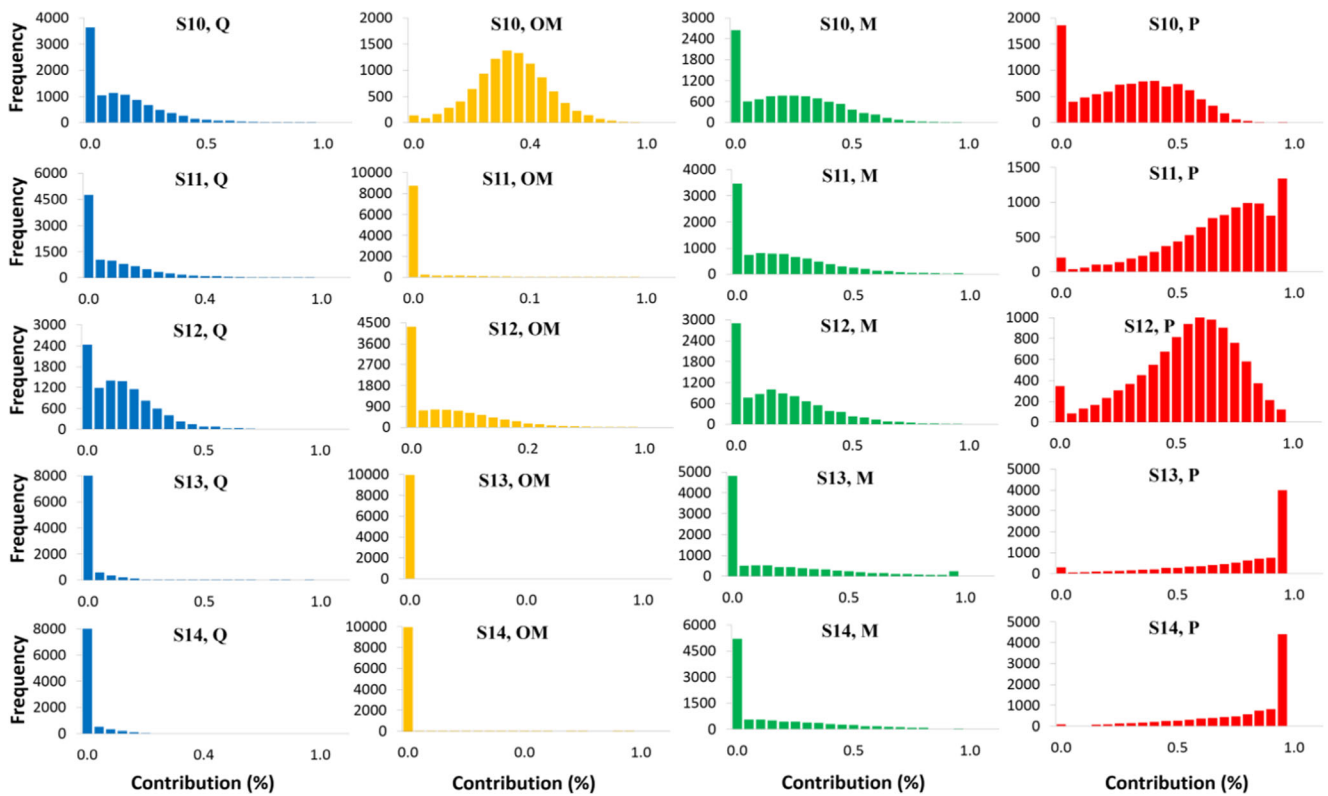


Fig. 11 Probability density functions of the Monte Carlo simulation results for estimating the sources of coarse-grained sediment in TSD samples (S10–S14)

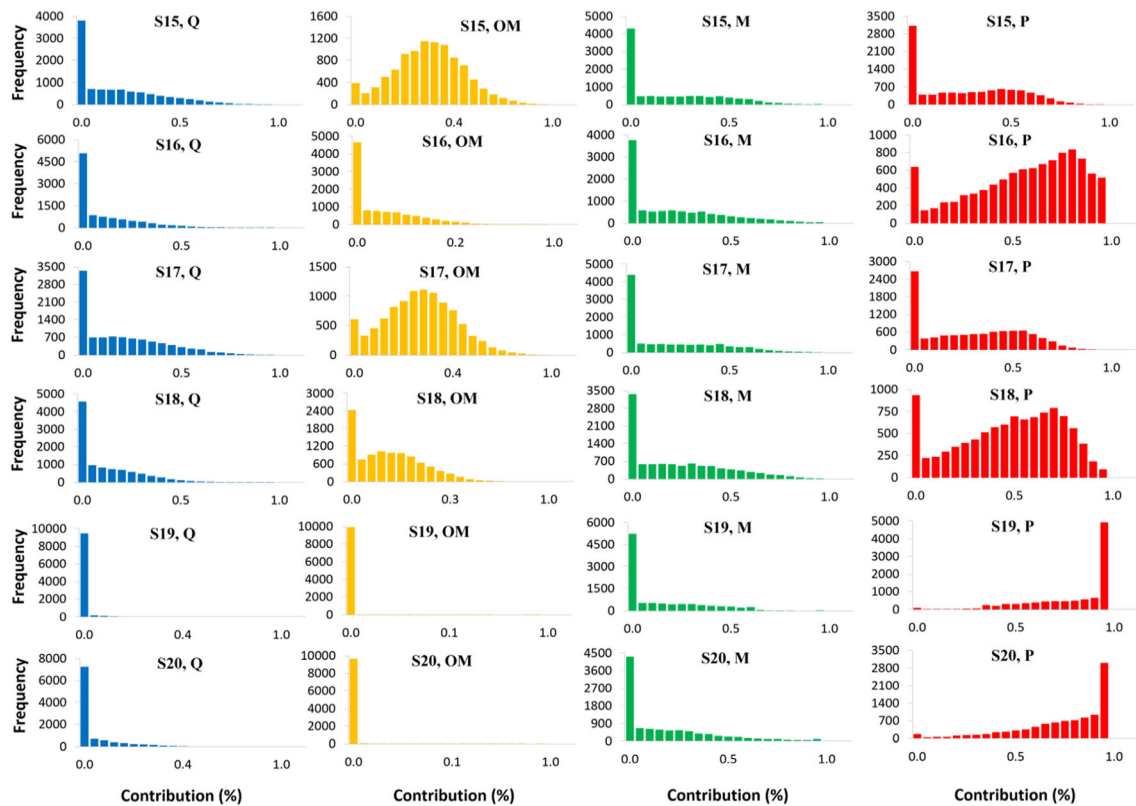


Fig. 12 Probability density functions of the Monte Carlo simulation results for estimating the sources of coarse-grained sediment in MD samples (S15–S20)

Table 6 Comparison of the modelled estimates of geological spatial source contributions for fine-grained and coarse-grained sediment fractions with known source proportions comprising six artificial sediment mixtures (S1–S6)

Virtual sediment sample no	Percentile (%)	Fine-grained fraction (< 63 μm)				Coarse-grained fraction (63–500 μm)			
		Geological spatial source				Geological spatial source			
		Q	OM	M	P	Q	OM	M	P
S1	2.5	0	0	0	0	0	5	0	0
	25	0	11	0	8	5	20	0	25
	50	14	22	17	34	15	27	14	40
	75	30	31	37	54	25	34	29	53
	97.5	81	70	90	100	51	49	61	70
	Average (%)	20	23	23	34	17	27	18	38
	Artificial sediment mixture (%)	25	25	25	25	25	25	25	25
S2	2.5	0	0	0	0	0	7	0	0
	25	0	13	0	5	2	22	0	27
	50	13	24	17	32	12	29	14	42
	75	29	33	38	52	22	35	29	54
	97.5	80	72	92	100	47	50	60	71
	Average (%)	19	25	23	33	14	29	18	39
	Artificial sediment mixture (%)	15	30	15	40	15	30	15	40
S3	2.5	0	0	0	0	0	0	0	0
	25	0	9	1	8	3	16	2	30
	50	10	19	22	35	13	23	16	45
	75	25	29	42	55	23	30	31	57
	97.5	73	87	100	100	48	44	62	75
	Average (%)	16	22	27	35	15	23	20	42
	Artificial sediment mixture (%)	20	20	40	20	20	20	40	20
S4	2.5	0	0	0	0	0	1	0	0
	25	3	7	0	9	9	18	0	21
	50	20	17	12	37	20	25	13	38
	75	37	27	32	56	31	33	29	51
	97.5	99	57	80	100	58	48	61	70
	Average (%)	25	19	20	36	21	26	18	35
	Artificial sediment mixture (%)	40	20	20	20	40	20	20	20
S5	2.5	0	0	0	0	0	15	0	0
	25	0	19	0	0	3	31	0	14
	50	11	31	15	24	14	38	13	30
	75	28	41	37	45	25	46	28	43
	97.5	78	82	97	100	50	62	58	61
	Average (%)	18	31	23	28	16	39	15	30
	Artificial sediment mixture (%)	20	40	20	20	20	40	20	40
S6	2.5	0	0	0	0	0	0	0	0
	25	0	7	0	12	3	15	1	33
	50	15	17	18	38	13	21	15	47
	75	31	26	38	57	23	28	29	59
	97.5	82	65	86	100	47	42	60	77
	Average (%)	20	19	23	38	15	22	18	45
	Artificial sediment mixture (%)	20	20	20	40	20	20	20	40

Table 7 Results of RMSE and MAE tests for evaluating the accuracy of the un-mixing model results using six artificial sediment mixtures (S1–S6)

Fraction	Test	Artificial sediment mixtures					
		S1	S2	S3	S4	S5	S6
< 63 μm	RMSE	5.6	6.3	10.3	11.1	6.25	2.3
	MAE	1.3	1	0.92	3.8	0.47	0.02
63–500 μm	RMSE	8.2	1.7	15.2	12.4	5	3.45
	MAE	2	0.2	1.2	4.7	1	1.2

be augmented with, or replaced by, alternative property types when tracing the sources of dust mobilized, redistributed and deposited in arid environments similar to the case study area. The testing of additional property types will inevitably require access to different laboratory equipment. Equally, the relatively low source sample discrimination rates again imply that tracer selection needs to be based on careful consideration of the environmental setting and sources in question and that the classification of potential sources should be explored in more depth using techniques including cluster analysis rather than being based on groups selected a priori (Pulley et al. 2017). The latter is relevant to the case study reported here in that the principal overlap between sources involved geological sources M (sandstone, siltstone, conglomerate, shale, mudstone, and shell beds; Darpahn and Jagin geological units; Miocene age deposits) and P (sandstone with siltstone, mudstone, and minor conglomerate; Palaeocene age deposits). Source discrimination and apportionment errors can also be improved by screening tracers on the basis of between-source to within-source group tracer concentration ratios.

Conclusions

Although there have been many studies of sand dunes of Quaternary age in both arid and semi-arid zones, much of the focus of previous research has been on genesis, sedimentary structures and the chronology of sand dunes. To date, there has been much less work on understanding dune sediment provenance, with many studies simply assuming an underlying rock or nearby sedimentary deposit as the primary source or ignoring the source issue altogether. Part of the reason that sand dune provenance studies are uncommon in aeolian geomorphology is that many of the techniques required are time-consuming, prone to operator error and highly specialized, often requiring expensive (some geochemical techniques) or sophisticated instrumentation (Muhs 2017; Muhs et al. 2017). Against this knowledge gap, this contribution has reported the results of fine-grained and coarse-grained

sediment fingerprinting, based on the application of a Monte Carlo simulation framework, in the coastal catchment of Jagin, south-east of Hormozgan province, southern Iran. The study area is impacted by many on-site and off-site effects of wind erosion, and research is needed to investigate practical mitigation options for aeolian dust transport and the costs involved. The preliminary results generated by this study, albeit in the context of the inherent limitations and uncertainties common to such work, underscore some of the challenges for this type of sediment fingerprinting application and provide some information for the targeting of mitigation options for wind erosion control. There is a need, however, for on the ground follow-up in the critical source areas to pinpoint the placement of control measures.

Acknowledgements The authors would like to thank the Faculty of Agriculture and Natural Resources, University of Hormozgan, Iran for supporting this joint research project.

Funding information Rothamsted Research receives strategic funding from the UK Biotechnology and Biological Sciences Research Council (BBSRC), and the input to this work by ALC was funded by grant BBS/E/C/00010330.

References

- Abban B, Papanicolaou AN, Cowles MK, Wilson CG, Abaci O, Wachha K, Schilling K, Schnobelen D (2016) An enhanced Bayesian fingerprinting framework for studying sediment source dynamics in intensively managed landscapes. *Water Resour Res* 52:4646–4673. <https://doi.org/10.1002/2015WR018030>
- Ahmady-Birgani H, Agahi E, Ahmadi SJ, Erfanian M (2018) Sediment source fingerprinting of the Lake Urmia sand dunes. *Sci Rep* 8(206): 1–15. <https://doi.org/10.1038/s41598-017-18027-0>
- Bernard PL, Foxgrover AC, Elias EPL, Erikson LH, Hein JR, McGann M, Mizell K, Rosenbauer RJ, Swarzenski PW, Takesue RK, Wong FL, Woodrow DL (2013) Integration of bed characteristics, geochemical tracers, current measurements, and numerical modeling for assessing the provenance of beach sand in the San Francisco Bay Coastal System. *Mar Geol* 345:181–206. <https://doi.org/10.1016/j.margeo.2013.08.007>
- Bottrill LJ, Walling DE, Leeks GJL (2000) Using recent overbank deposits to investigate contemporary sediment sources in larger river basins. In: Foster IDL (ed) *Tracers in geomorphology*. Wiley, Chichester, pp 369–387
- Brosinsky A, Foerster S, Segl K, Lopez-Tarazan JA, Pique G, Bronstert A (2014) Spectral fingerprinting: characterizing suspended sediment sources by the use of VNIR-SWIR spectral information. *J Soils Sediments*. <https://doi.org/10.1007/s11368-014-092-z>
- Carvalho C, Anjos RM, Veiga R, Macario K (2013) Application of radiometric analysis in the study of provenance and transport processes of Brazilian coastal sediments. *J Environ Radioact* 102:185–192. <https://doi.org/10.1016/j.jenvrad.2010.11.011>
- Cashman MJ, Gellis A, Sanisaca LG, Noe GB, Cogliandro V, Baker A (2018) Bank-derived material dominates fluvial sediment in a suburban Chesapeake Bay watershed. *River Res Applic* 1–13
- Chen F, Fang N, Shi Z (2016) Using biomarkers as fingerprint properties to identify sediment sources in a small catchment. *Sci Total Environ* 557-558:123–133

- Collins AL, Walling DE (2007) Sources of fine sediment recovered from the channel bed of lowland groundwater-fed catchments in the UK. *Geomorphology* 88:120–138. <https://doi.org/10.1016/j.geomorph.2006.10.018>
- Collins AL, Walling DE, Leeks GJL (1997) Fingerprinting the origin of fluvial suspended sediment in larger river basins: combining assessment of spatial provenance and source type. *Geogr Ann* 79:239–254
- Collins AL, Zhang Y, Walling DE, Grenfell SE, Smith P (2010) Tracing sediment loss from eroding farm tracks using a geochemical fingerprinting procedure combining local and genetic algorithm optimisation. *Sci Total Environ* 408(22):5461–5471. <https://doi.org/10.1016/j.scitotenv.2010.07.066>
- Collins AL, Zhang Y, McChesney D, Walling DE, Haley SM, Smith P (2012) Sediment source tracing in a lowland agricultural catchment in southern England using a modified procedure combining statistical analysis and numerical modelling. *Sci Total Environ* 414:301–317. <https://doi.org/10.1016/j.scitotenv.2011.10.062>
- Collins AL, Zhang YS, Duethmann D, Walling DE, Black KS (2013a) Using a novel tracing-tracking framework to source fine-grained sediment loss to watercourses at sub-catchment scale. *Hydrol Process* 27(6):959–974. <https://doi.org/10.1002/hyp.9652>
- Collins AL, Zhang Y, Hickinbotham R, Bailey G, Darlington S, Grenfell SE, Evans R, Blackwell M (2013b) Contemporary fine-grained bed sediment sources across the River Wensum Demonstration Test Catchment, UK. *Hydrol Process* 27:857–884
- Collins AL, Williams LJ, Zhang YS, Marius M, Dungait JAJ, Smallman DJ, ... Naden PS (2014) Sources of sediment-bound organic matter infiltrating spawning gravels during the incubation and emergence life stages of salmonids. *Agric Ecosyst Environ* 196:76–93. <https://doi.org/10.1016/j.agee.2014.06.018>
- Collins AL, Pulley S, Foster IDL, Gellis A, Porto P, Horowitz AJ (2017) Sediment source fingerprinting as an aid to catchment management: a review of the current state of knowledge and a methodological decision-tree for end-users. *J Environ Manag* 194:86–108. <https://doi.org/10.1016/j.jenvman.2016.09.075>
- Cooper RJ, Krueger T (2017) An extended Bayesian sediment fingerprinting mixing model for the full Bayes treatment of geochemical uncertainties. *Hydrol Process* 31:1900–1912. <https://doi.org/10.1002/hyp.11154>
- Cooper RJ, Krueger T, Hiscock KM, Rawlins BG (2014) Sensitivity of fluvial sediment source apportionment to mixing model assumptions: a Bayesian model comparison. *Water Resour Res* 50:9031–9047. <https://doi.org/10.1002/2014WR016194>
- Cooper RJ, Krueger T, Hiscock KM, Rawlins BG (2015) High-temporal resolution fluvial sediment source fingerprinting with uncertainty: a Bayesian approach. *Earth Surf Process Landf* 40(1):78–92. <https://doi.org/10.1002/esp.3621>
- Dahmardeh Behrooz R, Gholami H, Telfer MW, Jansen JD, Fathabadi A (2019) Using GLUE to pull apart the provenance of atmospheric dust. *Aeolian Res* 37:1–13. <https://doi.org/10.1016/j.aeolia.2018.12.001>
- Du S, Wu Y, Tan L (2018) Geochemical evidence for the provenance of aeolian deposits in the Qaidam Basin, Tibetan Plateau. *Aeolian Res* 32:60–70. <https://doi.org/10.1016/j.aeolia.2018.01.005>
- Evrard O, Lacey PJ, Huon S, Lefevre I, Sengtaheuanghoung O, Ribolzi O (2016) Combining multiple fallout radionuclides (^{137}Cs , ^7Be , $^{210}\text{Pbex}$) to investigate temporal sediment source dynamics in tropical ephemeral river systems. *J Soils Sediments* 16:1130–1144
- Franks SW, Rowan JS (2000) Multi-parameter fingerprinting of sediment sources: uncertainty estimation and tracer selection. *Comput Methods Water Resour* 13:1067–1074
- Franz C, Makeschin F, Weiß H, Lorz C (2014) Sediments in urban river basins: identification of sediment sources within the Lago Paranoá Catchment, Brasília DF, Brazil—using the fingerprint approach. *Sci Total Environ* 466–467:513–523. <https://doi.org/10.1016/j.scitotenv.2013.07.056>
- Gellis AC, Noe GB (2013) Sediment source analysis in the Linganore Creek watershed, Maryland, USA, using the sediment fingerprinting approach: 2008 to 2010. *J Soils Sediments* 13(10):1735–1753. <https://doi.org/10.1007/s11368-013-0771-6>
- Gholami H, Middleton N, NazariSamani AA, Wasson R (2017a) Determining contribution of sand dune potential sources using radionuclides, trace and major elements in central Iran. *Arabian J Geosci* 10:163. <https://doi.org/10.1007/s12517-017-2917-0>
- Gholami H, Telfer MW, Blake WH, Fathabadi A (2017b) Aeolian sediment fingerprinting using a Bayesian mixing model. *Earth Surf Process Landf* 42:2365–2376. <https://doi.org/10.1002/esp.4189>
- Habibi S, Gholami H, Fathabadi A, Jansen JD (2019) Fingerprinting sources of reservoir sediment via two modelling approaches. *Sci Total Environ* 663:78–96. <https://doi.org/10.1016/j.scitotenv.2019.01.327>
- Haddadchi A, Ryder D, Evrard O, Olley J (2013) Sediment fingerprinting in fluvial systems: review of tracers, sediment sources and mixing models. *Int J Sediment Res* 28:560–578. [https://doi.org/10.1016/S1001-6279\(14\)60013-5](https://doi.org/10.1016/S1001-6279(14)60013-5)
- Haddadchi A, Olley J, Lacey JP (2014) Accuracy of mixing models in predicting sediment source contributions. *Sci Total Environ* 497–498:139–152. <https://doi.org/10.1016/j.scitotenv.2014.07.105>
- Hein JR, Mizell K, Barnard PL (2013) Sand sources and transport pathways for the San Francisco Bay coastal system, based on X-ray diffraction mineralogy. *Mar Geol* 345:154–169. <https://doi.org/10.1016/j.margeo.2013.04.003>
- Hughes AO, Olley JM, Croke JC, McKergow LA (2009) Sediment source changes over the last 250 years in a dry-tropical catchment, central Queensland, Australia. *Geomorphology* 104:262–275
- Kairyte M, Stevens RL (2009) Quantitative provenance of silt and clay within sandy deposits of the Lithuanian coastal zone (Baltic Sea). *Mar Geol* 257:87–93. <https://doi.org/10.1016/j.margeo.2008.11.001>
- Koiter AJ, Lobb DA, Owens PN, Petticrew EL, Tiessen KHD, Li S (2013) Investigating the role of connectivity and scale in assessing the sources of sediment in an agricultural watershed in the Canadian prairies using sediment source fingerprinting. *J Soils Sediments* 13(10):1676–1691. <https://doi.org/10.1007/s11368-013-0762-7>
- Lahijani H, Tavakoli V (2012) Identifying provenance of South Caspian coastal sediments using mineral distribution pattern. *Quat Int* 261:128–137. <https://doi.org/10.1016/j.quaint.2011.04.021>
- Le Gall M, Evrard O, Foucher A, Lacey JP, Salvador-Blanes S, Thill O, Dapigny A, Lefèvre I, Cerdan O, Ayrault S (2016) Quantifying sediment sources in a lowland agricultural catchment pond using ^{137}Cs activities and radiogenic $^{87}\text{Sr}/^{86}\text{Sr}$ ratios. *Sci Total Environ* 566–567:968–980. <https://doi.org/10.1016/j.scitotenv.2016.05.093>
- Liu BL, Niu QH, Qu JJ, Zu RP (2016a) Quantifying the provenance of aeolian sediments using multiple composite fingerprints. *Aeolian Res* 22:117–122. <https://doi.org/10.1016/j.aeolia.2016.08.002>
- Liu B, Storm DE, Zhang XJ, Cao W, Duan X (2016b) A new method for fingerprinting sediment source contributions using distances from discriminant function analysis. *Catena* 147:32–39. <https://doi.org/10.1016/j.catena.2016.06.039>
- Manjoro M, Rowntree K, Kakembo V, Foster I, Collins AL (2016) Use of sediment source fingerprinting to assess the role of subsurface erosion in the supply of fine sediment in a degraded catchment in the Eastern Cape, South Africa. *J Environ Manag* 1–5. <https://doi.org/10.1016/j.jenvman.2016.07.019>
- Martínez-Carreras N, Udelhoven T, Krein A, Gallart F, Iffly JF, Ziebel J, Hoffmann L, Pfister L, Walling DE (2010) The use of sediment colour measured by diffuse reflectance spectrometry to determine sediment sources: application to the Attert River Catchment (Luxembourg). *J Hydrol* 382(1–4):49–63. <https://doi.org/10.1016/j.jhydrol.2009.12.017>
- Morshedi Nodej T, Rezazadeh M (2018) The spatial distribution of critical wind erosion centers according to the dust event in Hormozgan

- province (south of Iran). *Catena* 167:340–352. <https://doi.org/10.1016/j.catena.2018.05.008>
- Muhs DR (2017) Evaluation of simple geochemical indicators of Aeolian sand provenance: Late Quaternary dune fields of North America revisited. *Quat Sci Rev* 171:260–296. <https://doi.org/10.1016/j.quascirev.2017.07.007>
- Muhs DR, Prospero JM, Baddock MC, Gill TE (2014) Identifying sources of aeolian mineral dust: present and past, *Mineral Dust* (Book chapter). *Geosci Environ Change Sci Cent* 51–74. <https://doi.org/10.1007/978-94-017-8978-3>
- Muhs DR, Lancaster N, Skipp GL (2017) A complex origin for the Kelso Dunes, Mojave National Preserve, California, USA: a case study using a simple geochemical method with global applications. *Aeolian Res* 276:222–243. <https://doi.org/10.1016/j.geomorph.2016.10.002>
- Mukundan R, Walling DE, Gellis AC, Slattery MC, Radcliffe DE (2012) Sediment source fingerprinting: transforming from a research tool to a management tool. *J Am Water Resour Assoc* 48(6):1241–1257. <https://doi.org/10.1111/j.1752-1688.2012.00685.x>
- Nosrati K, Govers G, Ahmadi H, Sharifi F, Amoozegar MA, Merckx R, Vanmaercke M (2011) An exploratory study on the use of enzyme activities as sediment tracers: biochemical fingerprints. *Int J Sediment Res* 26:136–151
- Nosrati K, Collins AL, Madankan M (2018) Fingerprinting sub-basin spatial sediment sources using different multivariate statistical techniques and the modified MixSIR model. *Catena* 164:32–43
- Owens PN, Walling DE, Leeks GJL (1999) Use of floodplain sediment cores to investigate recent historical changes in overbank sedimentation rates and sediment sources in the catchment of the River Ouse, Yorkshire, UK. *Catena* 36:21–47
- Owens PN, Blake WH, Gaspar L, Gateuille D, Koiter AJ, Lobb DA, Petticrew EL, Reiffarth DG, Smith HG, Woodward JC (2016) Fingerprinting and tracing the sources of soils and sediments: Earth and ocean science, geoarchaeological, forensic, and human health applications. *Earth Sci Rev* 162:1–23. <https://doi.org/10.1016/j.earscirev.2016.08.012>
- Pham DT, Gouramanis C, Switzer AD, Rubin CM, Jones BG, Jankaew K, Carr PF (2018) Elemental and mineralogical analysis of marine and coastal sediments from Phra Thong Island, Thailand: insights into the provenance of coastal hazard deposits. *Mar Geol* 396:79–99. <https://doi.org/10.1016/j.margeo.2018.01.006>
- Prizomwala SP, Bhatt N, Basavaiah N (2014) Provenance discrimination and source-to-sink studies from a dryland fluvial regime: an example from Kachchh, western India. *Int J Sediment Res* 29:99–109
- Pulley S, Collins AL (2018) Tracing catchment fine sediment sources using the new SIFT (Sediment Fingerprinting Tool) open source software. *Sci Total Environ* 635:838–858
- Pulley S, Foster I, Collins AL (2017) The impact of catchment source group classification on the accuracy of sediment fingerprinting outputs. *J Environ Manag* 194:16–26
- Rao W, Tan H, Jiang S, Chen J (2011) Trace element and REE geochemistry of fine- and coarse-grained sands in the Ordos deserts and links with sediments in surrounding areas. *Chem Erde- Geochem* 71(2): 155–170. <https://doi.org/10.1016/j.chemer.2011.02.003>
- Rao W, Mao C, Wang Y, Su J, Balsam W, Ji J (2015) Geochemical constraints on the provenance of surface sediments of radial sand ridges off the Jiangsu coastal zone, East China. *Mar Geol* 359:35–49. <https://doi.org/10.1016/j.margeo.2014.11.007>
- Rao W, Mao C, Wang Y, Huang H, Ji J (2017) Using Nd-Sr isotopes and rare earth elements to study sediment provenance of the modern radial sand ridges in the southwestern Yellow Sea. *Appl Geochem* 81:23–35. <https://doi.org/10.1016/j.apgeochem.2017.03.011>
- Rosenbauer RJ, Foxgrover AC, Hein JR, Swarzenski PW (2013) A Sr–Nd isotopic study of sand-sized sediment provenance and transport for the San Francisco Bay coastal system. *Mar Geol* 345:143–153. <https://doi.org/10.1016/j.margeo.2013.01.002>
- Russell MA, Walling DE, Hodgkinson RA (2001) Suspended sediment sources in two small lowland agricultural catchments in the UK. *J Hydrol* 252(1–4):1–24. [https://doi.org/10.1016/S0022-1694\(01\)00388-2](https://doi.org/10.1016/S0022-1694(01)00388-2)
- Saitoh Y, Tamura T, Nakano T (2017) Geochemical constraints on the sources of beach sand, southern Sendai Bay, northeast Japan. *Mar Geol* 387:97–107. <https://doi.org/10.1016/j.margeo.2017.04.004>
- Stone M, Collins AL, Silins U, Emelko MB, Zhang YS (2014) The use of composite fingerprints to quantify sediment sources in a wildfire impacted landscape, Alberta, Canada. *Sci Total Environ* 473–474: 642–650. <https://doi.org/10.1016/j.scitotenv.2013.12.052>
- Tiecher T, Minella JPG, Evrard O, Caner L, Merten GH, Capoane V, Didone EJ, dos Santos DR (2018) Fingerprinting sediment sources in a large agricultural catchment under no-tillage in southern Brazil (Conceição River). *Land Degrad Dev* 29(4):939–951
- Voli MT, Wegmann KW, Bohnenstiehl DR, Leithold E, Osburn CL, Polyakov V (2013) Fingerprinting the sources of suspended sediment delivery to a large municipal drinking water reservoir: Falls Lake, Neuse River, North Carolina, USA. *J Soils Sediments* 13(10): 1692–1707. <https://doi.org/10.1007/s11368-013-0758-3>
- Walden J, Slattery MC, Burt TP (1997) Use of mineral magnetic measurements to fingerprint suspended sediment sources: approaches and techniques for data analysis. *J Hydrol* 202:353–372
- Walling DE (2013) The evolution of sediment source fingerprinting investigations in fluvial systems. *J Soils Sediments* 13(10):1658–1675. <https://doi.org/10.1007/s11368-013-0767-2>
- Walling DE, Owens PN, Leeks GJL (1999) Fingerprinting suspended sediment sources in the catchment of the River Ouse, Yorkshire, UK. *Hydrol Process* 13:955–975. [https://doi.org/10.1002/\(SICI\)1099-1085\(199905\)13:7<955::AID-HYP784>3.0.CO;2-G](https://doi.org/10.1002/(SICI)1099-1085(199905)13:7<955::AID-HYP784>3.0.CO;2-G)
- Wang G, Li J, Ravi S, Scott Van Pelt R, Costa PJM, Dukes D (2017) Tracer techniques in aeolian research: approaches, applications, and challenges. *Earth-Sci Rev* 170:1–16. <https://doi.org/10.1016/j.earscirev.2017.05.001>
- Weltje G (2012) Quantitative models of sediment generation and provenance: state of the art and future developments. *Sediment Geol* 280: 4–20
- Wilkinson S, Hancock G, Bartley R, Hawdon A, Keen R (2013) Using sediment tracing to assess processes and spatial patterns of erosion in grazed rangelands, Burdekin River basin, Australia. *Agric Ecosyst Environ* 180:90–102. <https://doi.org/10.1016/j.agee.2012.02.002>
- Wong FL, Woodrow DL, McGann M (2013) Heavy mineral analysis for assessing the provenance of sandy sediment in the San Francisco Bay Coastal System. *Mar Geol* 345:170–180. <https://doi.org/10.1016/j.margeo.2013.05.012>
- Zhang J, Yang M, Zhang F, Zhang W, Zhao T, Li Y (2017) Fingerprinting sediment sources after an extreme rainstorm event in a small catchment on the Loess Plateau, PR China. *Land Degrad Dev* 28:2527–2539
- Zular A, Sawakuchi AO, Guedes CCF, Giannini PCF (2015) Attaining provenance proxies from OSL and TL sensitivities: coupling with grain size and heavy minerals data from southern Brazilian coastal sediments. *Radiat Meas* 81:39–45. <https://doi.org/10.1016/j.radmeas.2015.04.010>

Publisher's note Springer Nature remains neutral with regard to jurisdictional claims in published maps and institutional affiliations.